Porous aromatic polyamides the easy and green way

Blanca S. Pascual, Miriam Trigo-López, José A. Reglero Ruiz, Jesús L. Pablos, Juan C. Bertolín, César Represa, José V. Cuevas, Félix C. García, José M. García

PII: S0014-3057(19)30294-0
DOI: https://doi.org/10.1016/j.eurpolymj.2019.03.058
Reference: EPJ 8960

To appear in: *European Polymer Journal*

Received Date: 13 February 2019
Revised Date: 25 March 2019
Accepted Date: 29 March 2019

Please cite this article as: Pascual, B.S., Trigo-López, M., Reglero Ruiz, J.A., Pablos, J.L., Bertolín, J.C., Represa, C., Cuevas, J.V., García, F.C., García, J.M., Porous aromatic polyamides the easy and green way, *European Polymer Journal* (2019), doi: https://doi.org/10.1016/j.eurpolymj.2019.03.058

Porous aromatic polyamides the easy and green way

Blanca S. Pascual,[1] Miriam Trigo-López,[1] José A. Reglero Ruiz,*[,1] Jesús L. Pablos,[2] Juan C. Bertolín,[3] César Represa,[3] José V. Cuevas,[1] Félix C. García,[1] and José M. García*[,1]

[1] Departamento de Química, Facultad de Ciencias, Universidad de Burgos, Plaza de Misael Bañuelos s/n, 09001 Burgos, Spain. Tel: +34 947 258 085; Fax: +34 947 258 831.

[2] Instituto de Ciencia y Tecnología de Polímeros, Consejo Superior de Investigaciones Científicas, ICTP-CSIC, Juan de la Cierva 3, 28006 Madrid, Spain. Tel: +34 915 622 900; Fax: +34 915 644 583.

[3] Departamento de Ingeniería Electromecánica, Área de Tecnología Electrónica, Escuela Politécnica Superior, Universidad de Burgos, Avda. Cantabria, s/n, 09006, Burgos, Spain. Tel: +34 947 258 900; Fax: +34 947 258 911.

* Corresponding author E-mails: jareglero@ubu.es; jmiguel@ubu.es

Abstract

We prepared microporous aramid films through a simple, inexpensive and green way, using ionic liquids (IL) as porosity promoters. Commercial poly(m-phenylene isophthalamide) (MPIA) films with different IL proportions were prepared, and then microporous films were obtained by removing the IL in distilled water. Microporous films presented density values between 0.34 and 0.71 g·cm^{-3} (around five times lower to commercial MPIA), with a homogeneous and controlled cellular morphology dependent on the proportion of the IL, showing cell sizes in the microcellular range (radii between 1 and 8 μm). Thermal, mechanical and electrical properties (specifically ionic conductivity) of the aramid films were analyzed to evaluate the influence of the IL proportion. Finally, it was observed that the MPIA/IL system presented a reversible thermally induced phase-separation process around 60 ºC, which was characterized through AFM-Raman images and spectra, together with the variation of the ionic conductivity.

Keywords: ionic liquid; aramid; porous film; thermally-induced phase separation

1. Introduction

Aromatic polyamides, also known as aramids, are polymers with excellent thermal and mechanical properties, and they are considered high performance materials. These materials first appeared in the patent literature in the late 1950s and early 60s with a number of compositions by DuPont researchers. However, the commercially important aramids nowadays is reduced to poly(*m*-phenylene isophthalamide) (MPIA) and poly(*p*-phenylen terephthalamide) (PPTA), due to their outstanding properties combined with their low density. [1] Current research efforts are directed into the improvement of the properties of these materials, [2] including lowering their weight without impairing their high-performance properties, which is important for applications related to the aeronautic and automotive industries and in human protection clothing. The preparation of polymers with cellular structure is a means for lowering the weight of materials. However, a vast control of their morphology is needed to produce these materials at an industrial scale, and thus, research efforts have been focused to reach that goal.

In our previous work, [3] we reported the development of foamed aramids using a non-volatile ionic liquid (1-allyl-3-methylimidazolium chloride) and supercritical CO_2 ($ScCO_2$) for the first time. We successfully lowered the density of commercial MPIA from 1.48 to 0.31 $g \cdot cm^{-3}$ while maintained the exceptional mechanical and thermal properties. $ScCO_2$ foaming process is widely employed to obtain micro and nanocellular polymers, due to the low critical conditions of $ScCO_2$ (31.1 °C and 73.8 bar), which offers many advantageous properties, like a tunable solvent power, plasticization of glassy polymers and higher diffusion rates. [4,5] On the contrary, the production of cellular polymers using $ScCO_2$ requires a specific experimental set-up, with a high-pressure reactor, and also high processing times (up to several hours), depending on the CO_2 affinity of the polymer.

We decided to explore the possibility of using ionic liquids due to their plasticization effect combined to their good affinity for the CO_2, two of the most important properties of these compounds. Traditionally, ionic liquids (IL) have been employed as green replacements for traditional volatile organic solvents as they are considered environmentally friendly and easily recyclable. [6] As a result, many examples can be found in aramids literature concerning the use of IL in many different applications, such as compatibilizers in composites, [7] as solvent for dry-jet-wet-electrospinning, [8] or as

solvents in the synthesis of PPTA or solution of its oligomers. [9,10] Furthermore, most of the ionic liquids are hygroscopic, [11,12] and they absorb water at different extents either from wet surfaces or from the air. [13-17] Concerning the specific relation between ionic liquids and aramids, we only found a work reported in 2007 about the use of different ionic liquids in the production of poly(*m*-phenylene isophtalamide) fibers. [18]

Although our initial goal was to evaluate the influence of the IL in the $ScCO_2$ foaming process, we surprisingly observed that only the removal of this specific IL to the aramid solution in dimethylacetamide (DMAc) during the preparation of cast films led to the development of a homogeneous microporous structure. In fact, when IL was removed, aramid films showed a high opacity, a classical effect of foamed materials, which is related to the diffraction of the light inside the microporous structure. The porosity could be explained through a thermally induced phase separation process due to the presence of the IL, a phenomenon described previously in the literature, [19,20] but which has not been reported as an alternative fabrication process of porous aramids. For this reason, we started this novel research line, which is presented in this work, focusing our efforts in the use of ILs to prepare microcellular aramids with controlled structure, avoiding the whole $ScCO_2$ foaming process, thus simplifying as much as possible the obtention of microporous aramid films.

Bearing these ideas in mind, we easily prepared five porous aramid films containing different proportions of ILs and a commercial dense MPIA film for comparison purpose, and we studied them in terms of cellular structure, density, mechanical, thermal and ionic conductivity measurements, evaluating the relation between the proportion of the IL added and the final characteristics of the microporous aramid films.

2. Experimental part

2.1. Materials and measurements

1-allyl-3-methylimidazolium chloride (≥ 97 %) was used as ionic liquid (Sigma-Aldrich, used as received). *N,N*-dimethylacetamide (DMAc, Aldrich, >99%) was vacuum-distilled over phosphorous pentoxide twice and then stored over 4 Å molecular sieves. Isophthalic dichloride (IPC) (Aldrich, >99%) was purified by double crystallization from dry heptane. m-Phenylenediamine (MPD) is commercially available (Aldrich, >99%) and was purified by double vacuum sublimation.

The number average molecular weight (M_w) of the polyamides was measured using the Mark-Houwink equation, $[\eta] = k\ M_w^{\alpha}$, where the values of the constant k and α for polymer solutions in 96% sulfuric acid are 0.00013 dL g^{-1} and 0.84, respectively. The intrinsic viscosity [η] was calculated by measuring the inherent viscosities, η_{inh}, of the aramid at different polymer concentrations (0.5, 0.3, 0.1 and 0.05 g·dL^{-1}) with a Ubbelohde viscometer using sulfuric acid (96%) as the solvent at 30 ºC ± 0.1 ºC and extrapolating to zero concentration.

Differential Scanning Calorimetry (DSC) measurements of the polyamide films were carried out in a DSC Q200 TA Instruments equipment. The analysis of the glass transition temperatures was carried out following a four-cycle procedure. First, after 5 min of stabilization at 30 °C, films were heated up to 350 °C at 20 °C/min. Then, after 5 min of stabilization at 350 °C, films were cooled down to RT at the same rate. Third, a second heating cycle was performed following the same conditions of the first cycle, concluding with a final cycle to cool down the samples to RT at 20 °C/min.

The AFM-RAMAN images and spectra were taken using a confocal AFM-RAMAN model Alpha300R – Alpha300A AFM Witec, using a laser wavelength of 532 nm with 2 mW, at 100X. The area of the image was fixed at 5x5 μm^2. Images and spectra were taken at RT and 70 °C. On the other hand, video images were recorded with the same equipment, at 10X, from RT to 70 °C, at a heating rate of 10 °C·min^{-1}, to observe the formation of the single MPIA-IL phase.

The thermogravimetric analysis data were recorded on a TA Instrument Q50 TGA analyzer. Films were first dried in vacuum overnight at 40 °C, and then TGA tests were performed under O_2 atmosphere using the next procedure: First, films were heated from RT to 100 °C at 10 °C·min^{-1}, and then kept during 5 min to eliminate the moisture content. Finally, TGA analysis was completed by heating up to 800 °C at 10 °C·min^{-1}.

To determine the mechanical properties 5x40 mm^2 strips were cut from the polyamide membrane and tensile tests were performed on a SHIMADZU EZ Test Compact Table-Top Universal Tester. Mechanical clamps were used and an extension rate of 5 mm·min^{-1} was applied using a gauge length of 9.44 mm. At least 5 samples were tested for each film, and the data was then averaged.

Cellular structural determination of the microcellular films was carried out in a scanning electron microscopy model JEOL JSM-6460LV. Films were frozen in liquid nitrogen, fractured and gold coated in vacuum to assure the electrical conductivity of the films.

Cellular structural characterization determining the average bubble radius and average cell density from SEM images, measured using the Image® software, counting the number of bubbles in each image n_i and its radius R_i. The average radius $\bar{R}$ is calculated from Equation 1:

$$\bar{R} = \frac{\sum_{i=1}^{N} n_i R_i}{\sum_{i=1}^{N} n_i} \quad (1)$$

where N represents the bubble count. Three different SEM images were analyzed from each material, averaging the data. The estimation of the cell density N_c was calculated using the Kumar's approximation, according to Equation 2:

$$N_c = \left(\frac{n}{A}\right)^{3/2} \quad (2)$$

where n is the number of cells in the image and A is the area of the image.

Taking into account the average radius value and cell density, the gas volume fraction V_f was obtained using Equation 3:

$$V_f = \frac{\pi \bar{d}^3 N_c}{6} \quad (3)$$

where $\bar{d}$ is the average diameter. Then, gas volume fraction V_f and foam density ρ^{SEM} are related throughout Equation 4, in which ρ_s is the solid material density:

$$V_f = 1 - \frac{\rho^{SEM}}{\rho_s} \quad (4)$$

The theoretical calculations were carried out using the quantum chemical software ORCA 4.0.1.2.1, using the PBEh-3c method. [21] This method, that shows excellent performance for non-covalent interaction energies in small and large complexes, includes geometrical counterpoise correction, gCP, [22] for removing the BSSE (Basis Set Superposition Error), and the atom-pairwise dispersion correction with the Becke-Johnson damping scheme (D3BJ). [23,24] The basis set used is def2-mSVP [25] in combination with auxiliary basis set RI-J. [26] Def2-mSVP is defined as the Valence double-zeta basis set of the Karlsruhe group with polarization function, whereas RI-J means the Resolution of Identity approximation (also called Density Fitting), applied to Coulomb Integrals (J). In this case, we are using the auxiliary basis def2/J. The Cartesian coordinates of the optimized geometries can be found in the ESI.

2.2. Preparation and testing of polyamide films

Aromatic polyamide MPIA was synthetized following the procedure described in our previous work by the conventional solution low temperature polycondensation method from IPC and MPD [27,28]. Thus, the polycondensation was carried out in a three necked flask fitted with a mechanical stirrer and nitrogen inlet. It was then charged with 39.40 mL of DMAc under a blanket of nitrogen at rt and 4.26 g (39.40 mmol) of MPD were added. After the solution of the diamine at rt under stirring, the system was then cooled to 0 °C, and 8.00 g (39.40 mmol) of IPC was added portion wise over 5 min (about four amounts). The reaction conditions were maintained for 30 min, and then the cooling was discontinued, and the reaction proceed for additional 3.5 h. The solution was slowly poured into distilled water, giving rise to a fibrous and swollen precipitate that was filtered, washed thoroughly with water and acetone. The yield was quantitative.

To prepare the porous aramid films with ILs a simple method was followed: 0.21 g of MPIA was dissolved portion wise in 3 mL of DMAc and stirred until full dissolution is observed. The corresponding amount of the IL was added then to the solution and stirred for an additional hour. After that, the mixture was filtered off and cast in a glass placed inside an air-circulating oven at 60 °C for 16 hours. To remove the ILs, the films were washed by immersing them in distilled water for 24 hours, replacing every 8 hours the distilled water solution to assure the complete removal of the IL. The tensile tests and the scanning electron microscopy images were obtained before and after removal the IL, whereas the thermal tests (TGA and DSC) were performed only after removing the IL. Finally, ionic resistivity tests were carried out in films containing the ILs.

3. Results and discussion

3.1. Preparation of aromatic polyamides

Aramids are high-performance polymers that are usually prepared in the lab using high and low temperature solution methods. The former from direct condensation of aromatic diacids and aromatic diamines, and the later by condensation of aromatic diacid dichlorides and aromatic polyamides. Commercially, these materials are synthesized following the low temperature methodology and processed into fibers (pulp, staple fibers, and continuous multifilament yarns) by dry-spinning, wet-spinning, and dry-jet wet-spinning [1]. In our case, we have prepared MPIA in solution upon polymerization IPC and MPDA (η_{inh} = 1.12 dL g^{-1}; [η] = 1.35 dL g^{-1}; M_w = 60 × 10^4).

For comparative studies we prepared a dense aromatic polyamide film was prepared by casting, called from now on dense MPIA, with a conventional density for aramids (1.43 g·cm^{-3}). Then, another five aramid films were prepared having 50, 60, 75, 80 and 90 % wt. of the IL 1-allyl-3-methylimidazolium chloride. It is important to remark that in a previous study, [3] lower percentages of IL were loaded to the polyamide, but no porous structure was observed.

3.2. Density and morphological parameters

After, we removed chemically the IL by immersion of the aramid films in distilled water for 24h. We denoted these films as 50MPIA/50LI-R, 40MPIA/60LI-R, 25MPIA/75LI-R, 20MPIA/80LI-R and 10MPIA/90LI-R. Then, the porous structure was originated due to the elimination of the IL in distilled water over 24h, causing the development of the porosity inside the polyamide film. **Figure S1** in the Electronic Supplementary Information (ESI) presents two photographs of the film containing 50 % of IL, before and after the IL removal process in distilled water during 24 h, in which an increase of the opacity of the film is evidenced, due to the formation of the microporous structure after the removal of the IL. To assure that all the DMAc and IL were completely removed after evaporating the solvent at 60 ºC during 16 h and lately placing the film in distilled water during 24 h, ^{1}H-RMN of the films were carried out using DMSO as solvent. **Figure S2** in the ESI presents, as an example, the ^{1}H-RMN spectrum of the 40MPIA/60LI-R film, in which no traces of DMAc or IL are observed. It is important to remark that the results were similar in all the films.

In **Table 1** we present the density of the microporous aramid films and the density of the dense MPIA film, together with the morphological parameters. In all the cases density vales are reduced compared to the dense film MPIA. Microporous aramid films present density values between 0.34 and 0.71 g·cm^{-3}, thus reaching a reduction between 2- and 4.5-times respect to the density of the dense MPIA. Concerning the morphology, all films present a well-defined microporous structure, with cell sizes between 1 and 8 µm, and cell densities in the range of 10^{8}-10^{11} cells·cm^{-3}. In addition, the film density was also estimated from the average cell size and cell density measurements (ρ^{SEM}), obtaining values which are comparable to the volumetric density, obtained directly from weight and geometrical dimensions, then validating the morphological calculation procedure.

Aramid Film	ρ	e	$\bar{R}$	N_c	V_f	ρ^{SEM}

	$(g \cdot cm^{-3})$	(μm)	(μm)	$(cells \cdot cm^{-3})$		$(g \cdot cm^{-3})$
Dense MPIA	1.43	27	n/a	n/a	n/a	n/a
50MPIA/50IL-R	0.71	66	1.64 ± 0.08	3.52×10^{11}	0.47	0.75
40MPIA/60IL-R	0.57	82	3.21 ± 0.23	4.41×10^{10}	0.57	0.61
25MPIA/75IL-R	0.38	171	8.32 ± 4.19	7.15×10^{8}	0.69	0.43
20MPIA/80IL-R	0.40	181	1.34 ± 0.18	1.37×10^{11}	0.70	0.42
10MPIA/90IL-R	0.34	269	n/a	n/a	n/a	n/a

Table 1. Morphological parameters of microporous aramid films. (ρ is the foam density measured from dimensions and weight of the film and e is the film thickness. ImageJ® software was employed to determine the average cell radius $\bar{R}$, the cell density N_C, the gas volume fraction V_f and the foam density from morphological parameters, ρ^{SEM}).

SEM micrographs of the cut section of the microporous aramid films were taken following the preparation procedure presented in section 2.1. **Figure 1** presents the micrographs taken on the cut section of the aramid films after the removal of the IL. On the other hand, different SEM images were taken of the surface of the aramid films, showing in all the cases a solid outer skin without any porosity (See **Figure S3** of the ESI).

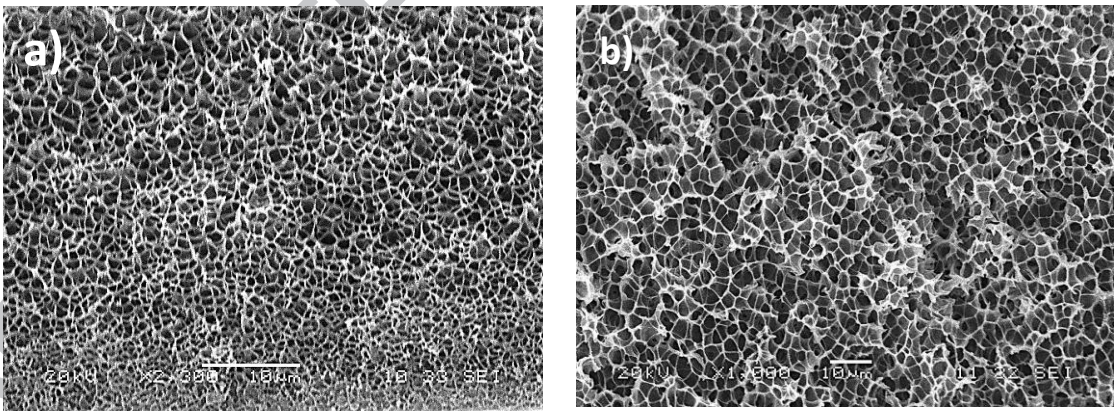

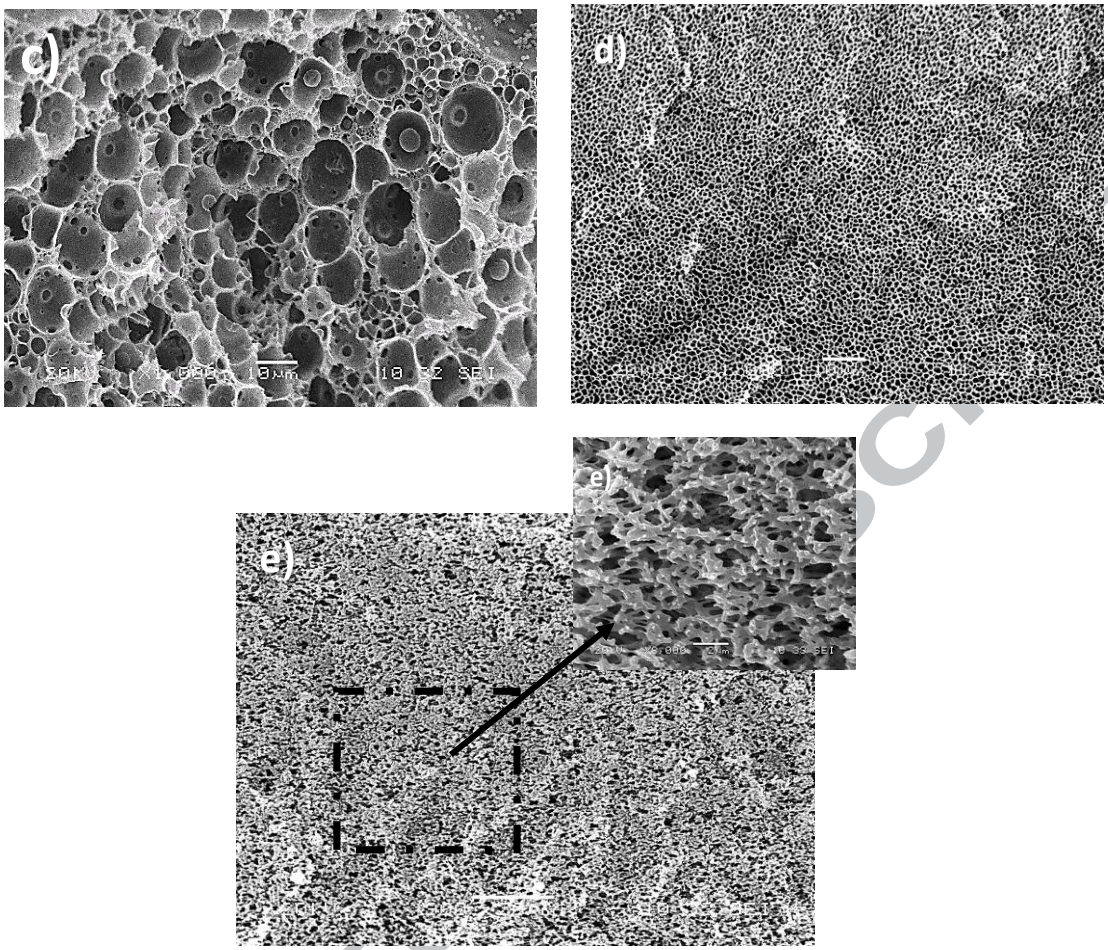

Figure 1. SEM micrographs of the microporous aramid films. All pictures taken at 1000x. a) 50MPIA/50IL-R; b) 40MPIA/60IL-R; c) 25MPIA/75IL-R; d) 20MPIA/80IL-R; e) 10MPIA/90IL-R (magnification taken at 3000x).

Having a look at the SEM micrographs in **Figure 1**, some specific conclusions can be extracted. Concerning the morphology of the microporous aramids, all the films prepared showed a very homogeneous structure with closed-cells. Only the aramid film with 90 % wt. of IL shows a very different morphology, with connected microchannels of a few microns width, in which the calculation of the different morphological parameters is not simple (see **Figure 1e**). This is probably due to the high proportion of the IL employed. The proportion of the IL is also crucial to control the average cell size. For example, there is a direct relation between the increase of cell size and the proportion of IL up to values of 75 % wt., but on the other hand, adding 80 % wt. of IL reduces drastically the cell size, then obtaining closed-cell microporous aramids with excellent homogeneity and cell sizes around 1 µm (see **Figure 1d**). These structures are specially interesting when compared to films with 75 % wt. of IL, which, although they are fabricated with almost the same quantity of IL, present a very inhomogeneous

structure, with bi-modal morphologies and also fractured cell walls (See **Figure 1c**). Several films were fabricated using the 75 % wt. of IL, obtaining the same inhomogeneous morphologies in all the cases, then confirming the very different behavior of this composition.

3.3. Thermally induced phase-separation process

Different literature works can be found in which ILs are used to obtain polymeric porous materials using several mechanisms. In this sense, a recent review analyzing the preparation of porous membranes for gas separation applications using ILs has been presented by Wang *et al.* [20] in 2016. Another interesting work was presented recently by Täuber *et al.* [29] in which porous polymer membranes were obtained from water soluble ionic liquids, via electrostatic complexation. Another fabrication route, based on the phase inversion process promoted by the ILs has been reported by Lakshmi *et al.* [30] as a very effective fabrication process of porous polyethersulfone membranes, using 1-butyl-3-methylimidazolium hexafluorophosphate as IL.

However, considering the specific fabrication of polymeric porous membranes using ILs as thermal phase-separation inducers, only a few works can be found in the literature. A classical review concerning the physic-chemical aspects of the phase-separation process in polymer solutions to produce porous membranes was presented by Van de Witte *et al.* [31] in 1996. More recently, different authors analyze the phase-separation process using ILs to obtain porous polymeric membranes. For example, Liu *et al.* [32] presented the preparation of porous poly(vinylidene fluoride) membranes using 1-butyl-2,3-dimethylimidazolium tetrafluoroborate as IL, and Chen *et al.* [33] showed the fabrication of porous poly(ethylene oxide) membranes employing 1-ethyl-3-methylimidazolium tetrafluoroborate as IL. Concerning the specific fabrication of porous aramid membranes, there is a lack of scientific literature up to date, due to the intrinsic difficulties associated to the production of these materials, then conferring to our work an excellent starting point to obtain porous aramid membranes.

As it has been commented in the introduction section, in our case, during the film preparation we observed that samples were transparent at 60 °C when they were extracted from the oven in which DMAc was evaporated, but after a few minutes at RT, the films turned completely opaque. We believe that the polyamide and the ionic liquid system (MPIA-IL) at 60 °C were completely mixed in a single phase, and then cooling down to RT caused the formation of a two-phase material via the phase-separation mechanism, originating the opacity. The phase-separation process is reversible, and

several heating-cooling cycles has been carried out changing from opaque to transparent samples when MPIA-IL phases were mixed or segregated, respectively.

The effect of the phase-separation process in the aramid films properties was investigated from different and complementary perspectives. In this section, we will focus our analysis in the AFM-Raman technique to study the IL distribution in the MPIA, and its relation to the microporous structure in the aramid film after the IL removal, following the protocol presented in section 2.1. The Raman analysis has been also previously employed by Lakshmi *et al.* [30], to analyze the distribution of 1-butyl-3-methylimidazolium hexafluorophosphate in polyethersulfone membranes. However, our objective was not only to analyze the distribution of the IL in the MPIA, but also to determine the relation between the IL presence and the microporous structure of the aramid film. The 50MPIA/50IL film was also selected as example, collecting two different Raman images and spectra (one at RT, in which both phases are clearly visible, and another at 70 °C, when a single-phase PA-IL is formed). **Figure 2** presents the obtained results.

The phase transition process is clearly demonstrated from the AFM Raman images and spectra taken at different temperatures. **Figure 2a** presents the Raman mapping taken from the 50MPIA/50IL at RT, in which both phases are separated, presenting each of the phases the Raman spectra of pure IL and pure MPIA. Heating the sample up to 70 °C leads to the formation of a single MPIA/IL phase, which is reflected in **Figure 2b**, in which the Raman mapping shows a homogeneous aspect, with a unique Raman spectrum corresponding to the mixed MPIA/IL phase. The formation of the single-phase is captured in **Figure S4** of the ESI, which shows several optical photographs of the 50MPIA/50IL film taken at different temperatures.

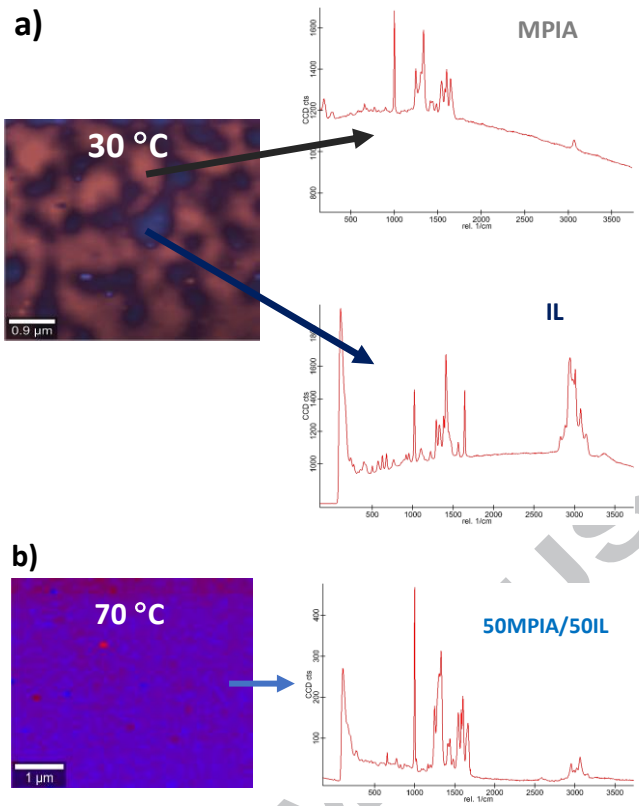

Figure 2. AFM Raman images and spectra of the 50MPIA/50IL film at different temperatures. a) 30 °C ; b) 70 °C.

As stated before, the formation of the microporous structure seems to be related to the removal of the IL, which could originate the porosity. **Figure S5** of the ESI presents the AFM Raman mapping taken at 30 °C of the 50MPIA/50IL film together with a SEM micrograph of the microporous 50MPIA/50IL-R after the IL removal, in which it is demonstrated that the IL distribution and the resultant porosity are directly related.

In order to get insight into the interaction of IL with the polymer, DFT calculations were performed (see experimental part for details). The structure of a polyamide dimer (mimicking the polymer structure) interacting with two ionic pairs of the IL, two interacting dimers, and an ionic liquid species were optimized. The two dimers display interactions of hydrogen bond and π-stacking between the two chains (see **Figure S6** of the ESI). The optimization of the dimer interacting with two ionic pairs of the ionic liquid displays how the chloride anions orientate towards the N-H bonds of the polyamide whereas the cationic 1-ethyl-3-methylimidazolium cation (IL) orientates towards the carboxylic oxygen of the polyamide (see **Figures S7** and **S8** in the ESI). The calculated free energy at 60 ºC for the reaction in which the two dimers interacts with the ionic liquid [$(polyamide)_2$ + 4 IL → 2 polyamide/$(IL)_2$] yields a value of -41.03 kcal·mol^{-1}, indicating that the interaction is thermodynamically favorable, in agreement

with experimental observation (the cartesian coordinates of the modelized structures are shown in the ESI, **Tables S1** to **S3**).

3.4. Thermal and mechanical properties

The key parameters of the aramids that makes them high performance materials are essentially the thermal and the mechanical behavior. The thermal behavior of the microporous films after the removal of the IL was evaluated in terms of 5 % and 10 % of weight loss through a thermogravimetric analysis (TGA), and the glass transition temperature (T_g) was determined with differential scanning calorimetry (DSC). Regarding the thermal resistance, the excellent performance of the commercial aromatic polyamides is practically maintained, with 5 % and 10 % weight loss around 430 °C and 460 °C (values of the dense MPIA film are 453 °C and 477 °C), regardless of the amount of ionic liquids, thus indicating that the removal of the ILs was practically completed. We only observed a small reduction of the thermal stability in film 25MPIA/75IL-R, (around 15 °C in $T_{5\%}$ and $T_{10\%}$ values), that could be related to the inhomogeneous microporous structure and the presence of fractured walls, as it was observed in the SEM micrograph presented in **Figure 1c**. Thus, it seems to be an influence of the microporous structure in the thermal stability of this aramid film, probably due to the different oxygen content trapped inside the cells, which can affect to the thermal resistance. Thermal properties are presented in **Table 2**. On the other hand, T_g values of the different films were maintained compared to the commercial MPIA, around 275 ºC. TGA and DSC curves of all aramid films can be found in **Figures S9** and **S10** of the ESI.

Aramid Film	$T_{5\%}$ (°C)	$T_{10\%}$ (°C)	T_g (°C)
Dense MPIA	453	477	273
50MPIA/50IL-R	438	462	271
40MPIA/60IL-R	438	465	275
25MPIA/75IL-R	423	438	276
20MPIA/80IL-R	433	466	275
10MPIA/90IL-R	431	463	276

Table 2. Thermal properties of aramid films. ($T_{5\%}$ and $T_{10\%}$ are the temperatures where 5 and 10 % wt. of mass loss, and T_g is the glass transition temperature)

The mechanical properties of the microporous aramid films were tested concerning the relative Young's moduli (E_r) and relative stress at break point (σ^{bp}_r), (ratio between measured values and film density, extracted from the data in **Table 1**). Relative values were employed in order to compare effectively the mechanical behavior of the microporous films and dense films obtained from commercial MPIA. All the stress-strain curves obtained in the tensile tests can be found in **Figure S11** of the ESI, whereas the mechanical data is presented in **Table 3**. (Mechanical data of dense MPIA film was extracted from our previous work. [3])

Aramid Film	E_r $(MPa\cdot(g\cdot cm^{-3})^{-1})$	σ^{bp}_r $(MPa\cdot(g\cdot cm^{-3})^{-1})$
Dense MPIA	1231 ± 47	53 ± 4
50MPIA/50IL-R	1013 ± 61	16 ± 4
40MPIA/60IL-R	922 ± 45	15 ± 1
25MPIA/75IL-R	490 ± 32	18 ± 3
20MPIA/80IL-R	1114 ± 59	15 ± 5
10MPIA/90IL-R	320 ± 23	12 ± 4

Table 3. Mechanical properties of aramid films obtained from the tensile tests. (E_r is the relative Young's modulus and σ^{bp}_r is the relative stress at break point).

Data presented in **Table 3** indicates a direct correlation between the microporous structure of the films and the relative mechanical values measured. As expected, the dense aramid film presents the best mechanical performance, with the highest values of both Young's modulus and stress at break relative values (1231 and 53 $MPa\cdot(g\cdot cm^{-3})^{-1}$, respectively). When microporous structure appears, there is a general reduction of the values of stress at break around four times, down to values between 12 and 18 $MPa\cdot(g\cdot cm^{-3})^{-1}$, then showing a ductile behavior compared to dense aramid film. However, the Young's modulus parameter does not follow the expected behavior, presenting some remarkable results, with a clear influence of the cell size and the homogeneity of the microporous structure. For example, in the case of the film 20MPIA/80IL-R, the relative Young's modulus lies around the value measured for the dense aramid film (1114 and 1231 $MPa\cdot(g\cdot cm^{-3})^{-1}$, respectively, indicating that it is possible to reduce the aramid's density from 1.43 to 0.40 $g\cdot cm^{-3}$ without losing mechanical resistance, then pointing out the role of the microporous structure created by simply eliminating the IL. On the contrary, we observed that the aramid microporous

film with 75 % wt. of IL (25MPIA/75IL-R) which presented a very inhomogeneous porous structure, with larger cell sizes and broken cell walls (see **Figure 1c**), shows a poor mechanical resistance, with values around 490 MPa·(g·cm^{-3})$^{-1}$. Both results indicate the influence of the microporous structure in the mechanical behavior of the aramid films, then giving the possibility of tuning easily their mechanical properties in terms of the initial proportion of IL employed.

3.5. Ionic conductivity

Ionic liquids are usually employed in the design of solid electrolytes with electrochemical characteristics comparable to those of liquid ones, in order to obtain self-standing materials combining high ionic diffusivity (and hence high ionic conductivity) and dimensional stability. For these reasons, in the last years the ideal candidates have been polymer-based materials in which the ionic diffusivity is enhanced with the presence of different ionic liquids, such as 1-ethyl-3-methylimidazolium bis(fluorosulfonyl)imide, 1-butyl-1-methylpyrrolidinium bis(fluorosulfonyl)imide or bis(trifluoromethane)sulfonimide lithium salt. [34,35]

Polyamides are essentially non-conductive materials, and they must be combined with different charges to obtain conducting materials with excellent mechanical and thermal properties. [36] In our case, we decided to analyze the ionic conductivity of the polyamide films using a four-point probe already employed in our group to determine the electrical properties of porous aramid films. [37] Films were cut in samples of 40x40 mm^2 and fixed to a glass plate. Then, the four-point probe was put in contact with the surface of the samples, obtaining the ionic resistivity. Five different measurements were carried out in each sample, to also observe the homogeneity of the surface, then averaging the results. **Figure 3** presents the ionic resistivity (ρ) obtained for each sample as a function of the proportion of ionic liquid.

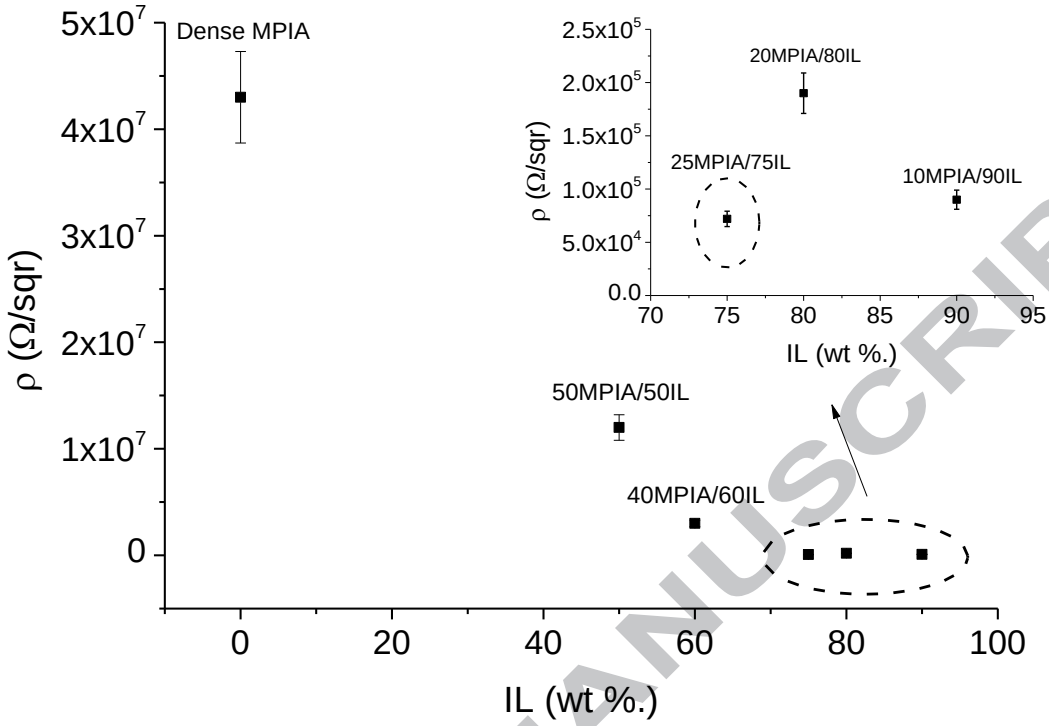

Figure 3. Ionic resistivity of porous aramids as a function of the quantity of ionic liquid.

The influence of the IL in the ionic transport properties of the aramid films is clearly observed in **Figure 3**. As expected, dense MPIA film shows a high ionic resistivity value due to the isolating behavior of the neat polymer. Increasing the quantity of the IL results in a decrease of the ionic resistivity, conferring a conductive behavior to the aramid films. Adding 50 % wt. of IL reduces four times the ionic resistivity compared to dense MPIA film (from $4 \cdot 10^7$ to $1 \cdot 10^7$ Ω/sqr). The reduction in the ionic resistivity is proportional to the quantity of IL, and, for example, aramid film with 90 % wt. of IL presents an ionic resistivity value around 10^5 Ω/sqr, then two magnitude orders lower than the dense MPIA. However, it is important to remark that measurement in aramid films with 90 % wt. were especially problematic, due to the great flexibility of the films the high quantity of IL, then hindering the contact between the tips of the probe and the surface of the material.

Additionally, aramid films with 75 % wt. do not seem to follow the expected correlation, presenting a very low value of the ionic resistivity (≈ $5 \cdot 10^4$ Ω/sqr), compared to films with 80 % wt (≈ $2 \cdot 10^5$ Ω/sqr). We already observed that this proportion of IL resulted in a very inhomogeneous cellular morphology (see **Figure 1c**), reflected also in the poor

tensile properties obtained (see **Figure S11** of the ESI). Thus, it seems that the proportion of the IL plays a key role in the resulting mechanical and ionic transport properties, demonstrating a direct relation microstructure-properties and opening the possibility of a controlled, simple and inexpensive fabrication of conductive aramid films with excellent mechanical properties.

To conclude, we also investigated the phase-separation process reversibility measuring the ionic resistivity during a heating-cooling cycle, using a controlled-temperature furnace. 50MPIA/50IL aramid sample was heated from RT to 80 °C and then cooling down to RT registering the ionic resistivity evolution. Results are presented in **Figure 4**. It can be observed that the ionic resistivity drops from $9{\cdot}10^6$ Ω/sqr to $2{\cdot}10^6$ Ω/sqr due to the formation of the single MPIA-IL phase between 50 and 70 °C. The reversibility is clearly demonstrated when aramid sample is cooled to RT and ionic resistivity recovers to $1.2{\cdot}10^7$ Ω/sqr. The difference between the initial resistivity and the value after the heating-cooling cycle could be due to a different distribution of the IL in the MPIA matrix, which affects to the ionic transport ability of the film. From these results, we can conclude that reversibility of the phase-separation process is directly reflected in the ionic conductivity of the aramid films, obtaining conductive aramid films when a single MPIA/IL phase is formed at temperatures around 60 °C.

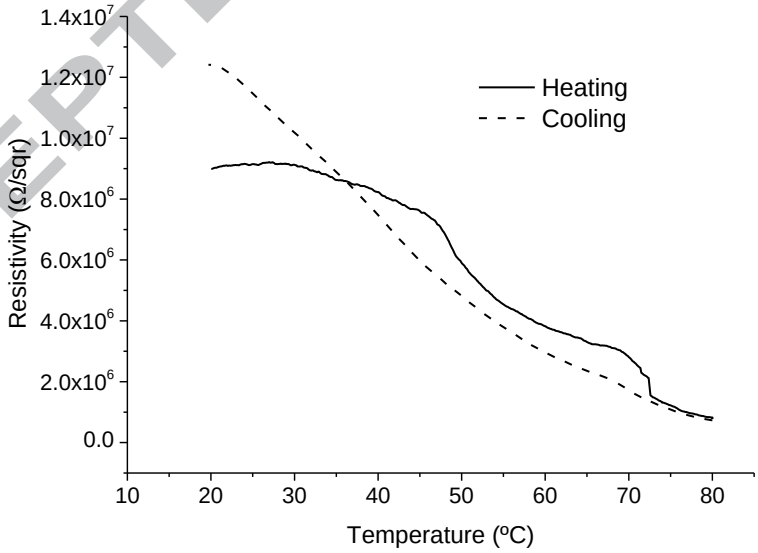

Figure 4. Ionic resistivity evolution in a heating-cooling cycle from RT to 80 °C in 50MPIA/50IL aramid film.

4. Conclusions

In short, we present an easy and inexpensive method to produce microporous aramid films with controlled morphology, adding ILs to commercial MPIA, which originated the microporous structure after removal in distilled water. Microcellular aramid films presented values of density between two and five times lower than dense MPIA. In addition, microporous morphology was controlled by the IL proportion, which was varied between 50 and 90 % wt., presenting in all the cases cell sizes below 8 µm.

Thermal properties of microporous films were analyzed from TGA and DSC measurements, finding that thermal resistance was maintained compared to dense MPIA film, then showing the positive effect of the microporous structure in low density films. Concerning the mechanical properties, tensile tests were carried out, showing that microporous aramid films presented a reduction of the values of stress at break value around four times, but on the other hand, Young's modulus parameter was surprisingly elevated, compared in relative terms to the value of the dense MPIA for samples with 80 % wt. of IL, then detecting a direct and clear influence of the cell size and the homogeneity of the microporous structure in the mechanical performance of the films. Ionic conductivity of the MPIA/IL films was also analyzed, detecting that the addition of the IL turned the MPIA film conductive.

Finally, we deeply investigated the reversible thermally-phase separation process associated to the presence of the IL in the MPIA matrix. It was observed that MPIA and IL formed a single phase around 60 ºC, detected in several experimental and theoretical ways: visually from different optical photographs taken at several temperatures, through AFM Raman images and spectra at different temperatures and also by measuring the evolution of the ionic resistivity in a heating-cooling cycle, finding that ionic resistivity decreased drastically due to the single-phase formation and turning the aramid film conductive. Also, numerical modelling confirmed that the reaction was thermodynamically favorable in good agreement with a strong interaction between the ionic liquid and the polyamide to form a single phase by heating up at 60 ºC, obtaining conductive aramid films when a unique MPIA/IL phase was formed, reversing the ionic transport ability when film was cooled to RT (two segregated MPIA/IL phases).

Acknowledgements

The financial support provided by FEDER (Fondo Europeo de Desarrollo Regional) and both the Spanish Agencia Estatal de Investigación (MAT2017-84501-R) and the Consejería de Educación-Junta de Castilla y León (BU306P18) is gratefully acknowledged. This research has made use of the high-performance computing

resources of the Castilla y León Supercomputing Center (SCAYLE, https://www.scayle.es), financed by FEDER (Fondo Europeo de Desarrollo Regional).

Funding

This research did not receive any specific grant from funding agencies in the public, commercial, or not-for-profit sectors.

References

[1] J.A. Reglero Ruiz, M. Trigo-López, F.C. García, J.M. García, Functional aromatic polyamides, Polymers. 9 (2017) 414. https://doi.org/10.3390/polym9090414.

[2] M. Trigo-López, J.M. García, J.A. Reglero, F.C. García, R. Ferrer, Aromatic polyamides, in: H.F. Mark (Ed.), Encyclopedia of Polymer Science and Technology, John Wiley & Sons, Inc., New Jersey, 2018, pp. 1-51.

[3] B.S. Pascual, M. Trigo-López, C. Ramos, M.T. Sanz, J.L. Pablos, F.C. García, J.A. Reglero Ruiz, J.M. García, Microcellular foamed aromatic polyamides (aramids). Structure, thermal and mechanical properties, Eur. Polym. J. 110 (2019) 9-13. https://doi.org/10.1016/j.eurpolymj.2018.11.007.

[4] A.I. Cooper, Porous materials and supercritical fluids, Adv. Mater. 16 (2003) 1049-1059. https://doi.org/10.1002/adma.200300380.

[5] J. Pinto, M. Dumon, M. Pedros, J.A. Reglero, M.A. Rodríguez-Pérez, Nanocellular CO_2 foaming of PMMA assisted by block copolymer nanostructuration, Chem. Eng. J. 243 (2014) 428-435. https://doi.org/10.1016/j.cej.2014.01.021.

[6] J.G. Huddleston, Characterization and comparison of hydrophilic and hydrophobic room temperature ionic liquids incorporating the imidazolium cation, Royal Soc. Chem. 3 (2001) 156-164. https://doi.org/10.1039/B103275P.

[7] V.D. Da Silva, M.M. Jacobi, H.S. Schrekker, S.C. Amico, Aramid pulp with physisorbed imidazolium ionic liquids for solvent-casted enhanced styrene-butadiene rubber composites, J. Appl. Polym. Sci. (2018) 46693. https://doi.org/10.1002/app.46693.

[8] W. Yang, H. Yu, M. Zhu, H. Bai, Y. Chen, Poly(*m*-phenylene isophthalamide) ultrafine fibers from an ionic liquid solution by dry-jet-wet-electrospinning, J. Macromol. Sci. B. 45 (2006) 573-579. https://doi.org/10.1080/00222340600770129.

[9] S. Dewilde, W. Dehaen, K. Binnemans, Ionic liquids as solvents for PPTA oligomers, Green Chem. 18 (2016) 1639-1652. https://doi.org/10.1039/C5GC02185E.

[10] S. Dewilde, T.V. Hoogerstraete, W. Dehaen, K. Binnemans, Synthesis of poly- *p*- phenylene terephthalamide (PPTA) in ionic liquids, ACS Sustainable Chem. Eng. 6 (2018) 1362-1369. https://doi.org/10.1021/acssuschemeng.7b03727.

[11] T. Köddermann, C. Wertz, A. Heintz, R. Ludwig, The association of water in ionic liquids: a reliable measure of polarity, Angew. Chem. Int. Ed. 45 (2006) 3697-3702. https://doi.org/10.1002/anie.200504471.

[12] Y. Cao, Y. Chen, X. Sun, Z. Zhang, T. Mu, Water sorption in ionic liquids: kinetics, mechanisms and hydrophilicity, Phys. Chem. Chem. Phys. 14 (2012) 12252-12262. https://doi.org/10.1039/C2CP41798G.

[13] I.H.J. Arellano, J.G. Guarino, F.U. Paredes, S.D. Arco, Thermal stability and moisture uptake of 1-alkyl-3-methylimidazolium bromide, J. Therm. Anal. Calorim. 103 (2011) 725-730. https://doi.org/10.1007/s10973-010-0992-5.

[14] J.G. Huddleston, A.E. Visser, W.M. Reichert, H.D. Willauer, G.A. Broker, R.D. Rogers, Characterization and comparison of hydrophilic and hydrophobic room temperature ionic liquids incorporating the imidazolium cation, Green Chem. 3 (2001) 156-164. https://doi.org/10.1039/B103275P.

[15] K.R. Seddon, A. Stark, M.J. Torres, Influence of chloride, water and organic solvents on the physical properties of ionic liquids, Pure Appl. Chem. 72 (2000) 2275-2287. https://doi.org/10.1351/pac200072122275.

[16] L. Cammarata, S. Kazarian, P. Salter, T. Welton, Molecular states of water in room temperature ionic liquids, Phys. Chem. Chem. Phys. 3 (2001) 5192-5200. https://doi.org/10.1039/B106900D.

[17] S. Cuadrado-Prado, M. Domínguez-Pérez, E. Rilo, S. García Garabal, L. Segade, C. Franjo, O. Cabeza, Experimental measurement of the hygroscopic grade on eight imidazolium based ionic liquids, Fluid Phase Equilib. 278 (2009) 36-40. https://doi.org/10.1016/j.fluid.2008.12.008.

[18] T. Zhao, W. Wang, Y. Zhang, B. Wang, J. Jiang, The preparation and characterization of poly(*m*-phenylene-isophthalamide) fibers using ionic liquids, Int. J. Mol. Sci. 8 (2007) 680-685. https://doi.org/10.3390/i8070680.

[19] T. Ueki, M. Watanabe, Macromolecules in ionic liquids: progress, challenges, and opportunities, Macromolecules 41 (2008) 3739-3749. https://doi.org/10.1021/ma800171k.

[20] J. Wang, J. Luo, S. Feng, H. Li, H. Wan, X. Zhang, Recent development of ionic liquid membranes, Green Energy & Environment 1 (2016) 43-61. https://doi.org/10.1016/j.gee.2016.05.002.

[21] F. Neese, The ORCA program system, Wiley Interdiscip. Rev. Comput. Mol. Sci. 2 (2012) 73–78. https://doi.org/10.1002/wcms.81.

[22] S. Grimme, J.G. Brandenburg, C. Bannwarth, A. Hansen, Consistent structures and interactions by density functional theory with small atomic orbital basis sets, J. Chem. Phys. 143 (2015) 54107. https://doi.org/10.1063/1.4927476.

[23] H. Kruse, S.A. Grimme, A geometrical correction for the inter- and intra-molecular basis set superposition error in Hartree-Fock and density functional theory calculations for large systems, J. Chem. Phys. 136 (2012) 154101. https://doi.org/10.1063/1.3700154.

[24] S. Grimme, J. Antony, S. Ehrlich, H. Krieg, A consistent and accurate ab initio parametrization of density functional dispersion correction (DFT-D) for the 94 elements H-Pu, J. Chem. Phys. 132 (2010) 154104. https://doi.org/10.1063/1.3382344.

[25] F. Weigend, R. Ahlrichs, Balanced basis sets of split valence, triple zeta valence and quadruple zeta valence quality for H to Rn: design and assessment of accuracy, Phys. Chem. Chem. Phys. 7 (2005) 3297–3305. https://doi.org/10.1039/B508541A.

[26] F. Weigend, Accurate Coulomb-fitting basis sets for H to Rn, Phys. Chem. Chem. Phys. 8 (2006) 1057-1065. https://doi.org/10.1039/b515623h.

[27] M. Trigo-López, A. Miguel-Ortega, S. Vallejos, A. Muñoz, D. Izquierdo, A. Colina, F.C. García, J.M. García, Intrinsically colored wholly aromatic polyamides (aramids), Dyes Pigments 122 (2015) 177-183. https://doi.org/10.1016/j.dyepig.2015.06.027.

[28] M. Trigo-López, J.L. Barrio-Manso, F. Serna, F.C. García, J.M. García, Crosslinked aromatic polyamides: A further step in high-performance materials, Macromol. Chem. Phys. 214 (2013) 2223-2231. https://doi.org/10.1002/macp.201300342.

[29] K. Täuber, A. Zimathies, J. Yuan, Porous membranes built up from hydrophilic poly(ionic liquid)s, Macromol. Rapid Commun. 36 (2015) 2176-2180. https://doi.org/10.1002/marc.201500480.

[30] S. Lakshmi, T. Cundari, E. Furia, A. Tagarelli, G. Fiorani, M. Carraro, A. Figoli, Preparation of polymeric membranes and microcapsules using an ionic liquid as morphology control additive, Macromol. Symp. 357 (2015) 159-167. https://doi.org/10.1002/masy.201400214.

[31] P. Van de Witte, P.J. Dijkstra, J.W.A. Van den Berg, J. Feijen, Phase separation processes in polymer solutions in relation to membrane formation, J. Membr. Sci. 117 (1996) 1-31. https://doi.org/10.1016/0376-7388(96)00088-9.

[32] Z. Liu, D. Sun, W. Dong, S. Feng, C. Xiao, Y. Zhang, J. Wei, Poly(vinylidene fluoride) (PVDF) membrane preparation with an ionic liquid via thermally induced phase separation melt technology, Applied Mechanics and Materials 694 (2014) 462-465. https://doi.org/10.4028/www.scientific.net/AMM.694.462.

[33] Y. Chen, Y. Niu, P. Gong, Z. Xiao, G. Li, Thermally reversible and irreversible phase transition behaviors in poly(ethylene oxide)/ionic liquid mixtures, Macromol. Rapid Commun. 38 (2017) 1700401. https://doi.org/10.1002/marc.201700401.

[34] J.L. Pablos, N. García, L. Garrido, J. Guzmán, F. Catalina, T. Corrales, P. Tiemblo, Highly efficient mixed Li^+ transport in ion gel polycationic electrolytes, J. Membr. Sci. 545 (2018) 133-139. https://doi.org/10.1016/j.memsci.2017.08.073.

[35] V.V. Zuev, Y.G. Ivanova, Mechanical and electrical properties of polyamide-6-based nanocomposites reinforced by fulleroid fillers, Polym. Eng. Sci. 52 (2012) 1206-1211. https://doi.org/10.1002/pen.22188.

[36] A. Dasari, Z-Z. Yu, Y-W. Mai, Electrically conductive and super-tough polyamide-based nanocomposites, Polymer 50 (2009) 4112-4121. https://doi.org/10.1016/j.polymer.2009.06.026.

[37] B.S. Pascual, S. Vallejos, J.A. Reglero Ruiz, J.C. Bertolín, C. Represa, F.C. García, J.M. García, Easy and inexpensive method for the visual and electronic detection of oxidants in air by using vinylic films with embedded aniline, J. Hazard. Mater. 364 (2019) 238-243. https://doi.org/10.1016/j.jhazmat.2018.10.039.

Graphical abstract

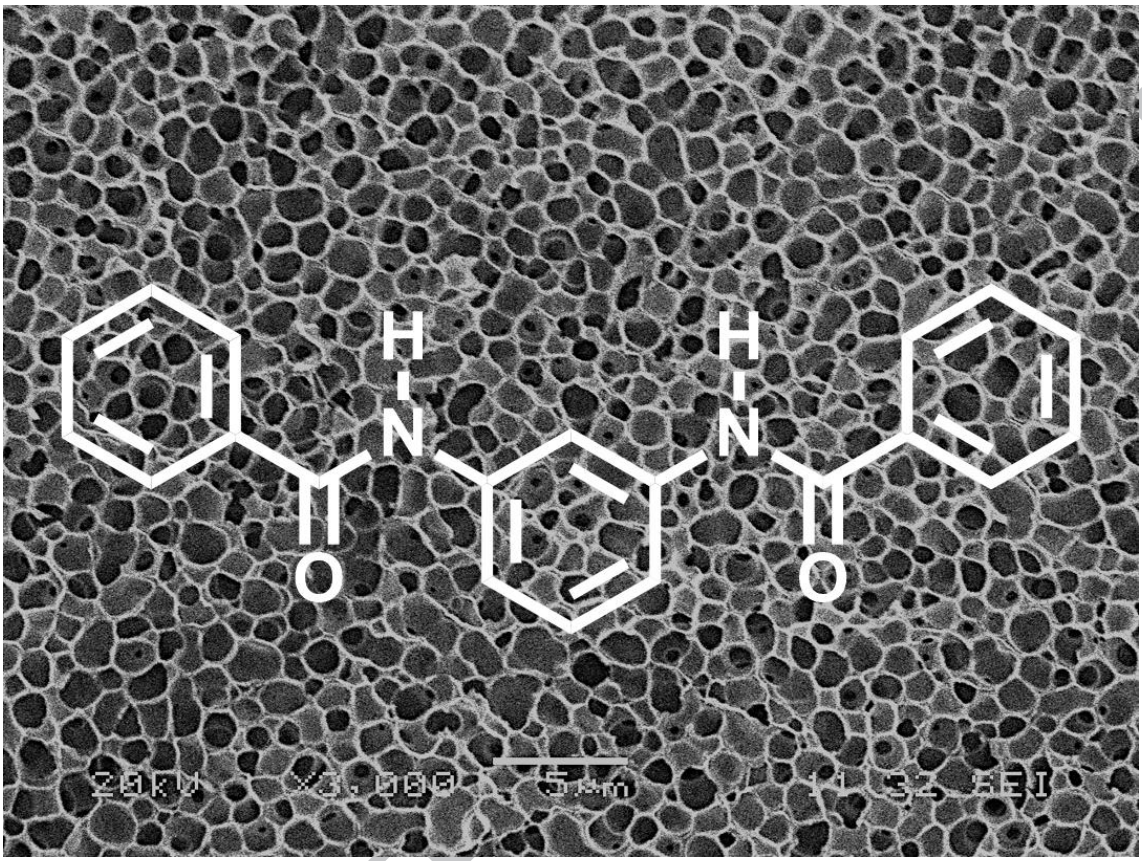

Highlights

- Microcellular aramid films have been obtained using exclusively ionic liquids
- Density has been diminished from 1.4 g·cm^{-3} down to 0.37 g·cm^{3}
- Average cell size lies in the microcellular range (between 1 and 8 μm)
- Cellular morphology can be controlled through the ionic liquid proportion
- Thermally induced phase-separation process has been investigated